

Nitrogen- and Fluorine-Doped Carbon Nanohorns as Efficient Metal-Free Oxygen Reduction Catalyst:  
Role of the Nitrogen Groups

*Original*

Nitrogen- and Fluorine-Doped Carbon Nanohorns as Efficient Metal-Free Oxygen Reduction Catalyst: Role of the Nitrogen Groups / Tosin, Elisa; Gatti, Teresa; Agnoli, Stefano; Calvillo, Laura; Menna, Enzo. - In: SURFACES. - ISSN 2571-9637. - 6:3(2023), pp. 227-238. [10.3390/surfaces6030015]

*Availability:*

This version is available at: 11583/2980249 since: 2023-07-13T07:21:17Z

*Publisher:*

MDPI

*Published*

DOI:10.3390/surfaces6030015

*Terms of use:*




This article is made available under terms and conditions as specified in the corresponding bibliographic description in the repository

*Publisher copyright*

(Article begins on next page)

## Article

# Nitrogen- and Fluorine-Doped Carbon Nanohorns as Efficient Metal-Free Oxygen Reduction Catalyst: Role of the Nitrogen Groups

Elisa Tosin <sup>1</sup>, Teresa Gatti <sup>1,2</sup> , Stefano Agnoli <sup>1</sup>, Laura Calvillo <sup>1,\*</sup>  and Enzo Menna <sup>1,3,\*</sup> 

<sup>1</sup> Department of Chemical Sciences, University of Padua, Via Marzolo 1, 35131 Padova, Italy

<sup>2</sup> Department of Applied Science and Technology, Politecnico di Torino, Corso Duca degli Abruzzi 24, 10129 Torino, Italy

<sup>3</sup> Interdepartmental Centre Giorgio Levi Cases for Energy Economics and Technology, University of Padua, 35131 Padua, Italy

\* Correspondence: laura.calvillolamano@unipd.it (L.C.); enzo.menna@unipd.it (E.M.); Tel.: +39-049-827-5122 (L.C.); +39-049-827-5660 (E.M.)

**Abstract:** The search of active, stable and low costs catalysts for the oxygen reduction reaction (ORR) is crucial for the extensive use of fuel cells and metal–air batteries. The development of metal-free catalysts, instead of platinum-based materials, can dramatically reduce the cost and increase the efficiency of these devices. In this work, carbon nanohorns (CNHs) have been covalently functionalized with N-containing heterocycles by the Tour reaction protocol and tested as metal-free ORR catalysts. The insertion of N-functionalities favored the complete reduction of oxygen to hydroxyl ions, while their absence favored the production of hydrogen peroxide. With the aim of determining the N-species responsible for the ORR activity of CNHs, photoemission and electrochemical measurements were combined. Results suggest that protonated N is the main species involved in the ORR process, facilitating the adsorption of oxygen, with their consequent reduction to neutral hydrogenated N species.

**Keywords:** carbon nanohorns; nitrogen groups; oxygen reduction reaction; in line XPS



**Citation:** Tosin, E.; Gatti, T.; Agnoli, S.; Calvillo, L.; Menna, E. Nitrogen- and Fluorine-Doped Carbon Nanohorns as Efficient Metal-Free Oxygen Reduction Catalyst: Role of the Nitrogen Groups. *Surfaces* **2023**, *6*, 227–238. <https://doi.org/10.3390/surfaces6030015>

Academic Editor: Pasquale Fernando Fulvio

Received: 12 May 2023

Revised: 28 June 2023

Accepted: 6 July 2023

Published: 8 July 2023



**Copyright:** © 2023 by the authors. Licensee MDPI, Basel, Switzerland. This article is an open access article distributed under the terms and conditions of the Creative Commons Attribution (CC BY) license (<https://creativecommons.org/licenses/by/4.0/>).

## 1. Introduction

Alkaline fuel cells (AFCs) and rechargeable metal–air batteries (MABs) are next-generation energy devices for clean power generation [1–4]. However, the improvement of their efficiencies as well as the reduction in their costs are crucial for their extensive use, both in stationary and mobile applications, which would facilitate the transition to a more sustainable future. Both devices have in common the electrochemical reaction that takes place at the cathode side during the discharge process, which is the oxygen reduction reaction (ORR) in an alkaline environment. The alkaline character of the electrolyte allows for the use of non-noble metals or even metal-free catalysts, instead of platinum-based materials, which can dramatically reduce the costs and increase the efficiency of the electrochemical devices.

Carbon materials have been extensively studied as a new class of metal-free ORR catalysts [5–7]. There exists a wide range of carbon materials with different properties, such as activated carbon, graphite, graphene, fullerene, carbon black, carbon nanotubes (CNTs), etc., and most of them have been tested as ORR catalysts [8–10]. In particular, doped carbon materials have attracted much attention since it has been demonstrated that the doping of carbon materials with more electronegative atoms, such as nitrogen, phosphorus, and sulfur, creates a positive charge density on adjacent carbon atoms that facilitates oxygen adsorption and charge transfer [10–12]. Nitrogen, in particular, has been widely studied due to its suitable atomic size and electronegativity [9,13,14]. Nitrogen-doped carbon materials

usually contain different nitrogen species, which are expected to present a different ORR activity. The role of these species has already been investigated, however, there is still a big controversy on which species are involved in the ORR mechanism. In the literature, some groups defend that pyridinic N species are the active ones [13–16], whereas other groups attribute the activity of this type of materials to graphitic N species [17–19].

In this work, we have studied carbon nanohorns (CNHs) covalently functionalized with N-containing heterocycles as metal-free ORR catalysts. CNHs are conical carbon nanostructures constructed from an  $sp^2$  carbon sheet. Their special morphology and graphitic structure provide them with suitable properties for electrochemical applications [20]. However, they have been less investigated than other carbon materials, such as CNTs or graphene [14,21,22].

We have decorated the CNHs with nitrogen functionalities by chemical functionalization through the Tour reaction protocol [23]. As reported by Giambastiani and coworkers, this is an effective method to prepare metal-free carbon-based catalysts with excellent ORR catalytic activity [13]. In addition to the physicochemical and electrochemical characterization of the functionalized carbon materials, here we present an in situ study of the evolution of nitrogen functionalities under ORR conditions in order to shine light on their role and involvement in the ORR mechanism. Our results support that protonated N species facilitate oxygen adsorption and are the ones involved in the actual ORR.

## 2. Materials and Methods

### 2.1. Materials

All reagents and solvents were purchased from Sigma-Aldrich (Milan, Italy) and used as received if not otherwise specified. Single-walled CNHs were purchased from Carbonium s.r.l. (Padua, Italy) and present a dahlia-type shape with a diameter of 60–120 nm. Electron microscopy evidence of the structure and morphology of the CNHs used in this work can be found in the literature [24–26].

### 2.2. Synthesis of Functionalized Carbon Nanohorns (CNHs)

**CNH-Py-Br.** As-purchased CNHs (8.3 mg, 0.69 mmol of C) have been dispersed in 1-cyclohexyl-2-pyrrolidone (CHP, 7.0 mL) through pulsed sonication for 10 min and transferred in a two-necked round-bottomed flask. A solution of 4-amino-2-bromopyridine (142.4 mg, 0.82 mmol) in 3 mL of CHP was added, and the mixture was heated to 80 °C under a nitrogen atmosphere. Then, isopentyl nitrite (100 µL, 0.74 mmol) was added carefully. After 15 min of continuous stirring, the reaction mixture was diluted with cold methanol (100 mL) and filtered through a PTFE membrane filter (Fluoropore, 0.22 µm pore size). The filtrate was washed with methanol (4 × 20 mL) and dried under an IR lamp for 15 min.

The product was dispersed in  $CHCl_3$  (7 mL) through pulsed sonication (5 min) followed by centrifugation (4500 rpm, 15 min, 20 °C). The supernatant was recovered and characterized.

**CNH-Py-F.** As-purchased CNHs (9.3 mg, 0.77 mmol of C) have been dispersed in CHP (7.0 mL) through pulsed sonication for 10 min and transferred in a two-necked round-bottomed flask. A solution of 4-amino-2-fluoropyridine (93.4.0 mg, 0.83 mmol) in 3 mL of CHP was added, and the mixture was heated to 80 °C under a nitrogen atmosphere. Then, isopentyl nitrite (100 µL, 0.74 mmol) was added carefully. After 15 min of continuous stirring, the reaction mixture was diluted with cold methanol (100 mL) and filtered through a PTFE membrane filter (Fluoropore, 0.22 µm pore size). The filtrate was washed with methanol (4 × 20 mL) and dried under an IR lamp for 15 min.

### 2.3. Physicochemical Characterization

Each product was dispersed in  $CHCl_3$  (7 mL) through pulsed sonication (5 min) followed by centrifugation (4500 rpm, 15 min, 20 °C). The supernatant was recovered and characterized.

Thermogravimetric analysis (TGA) was carried out using a Q5000IR TGA (TA Instruments, New Castle, DE, USA) under nitrogen by an isotherm at 100 °C for 10 min followed by heating at 10 °C/min rate until 1000 °C.

DLS measurements were carried out on a Zetasizer Nano S (Malvern Instruments, Malvern, UK), setting the material as polystyrene latex (RI = 1.590, Abs = 0.010) and the measurement angle at 173°, backscatter (NIBS default). DLS analyses were carried out in CHCl<sub>3</sub> at 25 °C (equilibration time = 120 s), performing 3 measurements of 11 runs with run duration set at 10 s for each measurement and using quartz cuvettes, according to the solvent, with a 1 cm optical path. Kinetic analysis was performed, collecting 60 measurements (11 runs with run duration set at 10 s each) with 600 s delay between measurements.

Raman spectra of samples drop-casted on precleaned glass micro slides (Corning, Corning, NY, USA) and dried under vacuum were recorded using an Invia (Renishaw, Wotton-under-Edge, UK) Raman microspectrometer (50 × objective) using the 633 nm line of a He–Ne laser at room temperature with a low laser power (<1 µW).

Pulsed sonication was carried out using a S-3000 sonicator (Misonix, Farmingdale, NY, USA) equipped with a titanium tip (power level: 2.0, pulse on: 3 s, pulse off: 3 s).

Centrifugations were carried out using a MR23i centrifuge (Thermo Electron Corporation, Waltham, MA, USA) with a varying angle rotor (model 11174711/11174720).

X-ray photoelectron spectroscopy (XPS) measurements were acquired in a custom-made UHV system working at a base pressure of 10<sup>−10</sup> mbar, equipped with an EA125 electron analyzer (Omicron Taunusstein, Germany) and an X-ray source with a dual Al–Mg anode. Core-level photoemission spectra (C 1s, N 1s, O 1s, F 1s, and Br 3d regions) were collected in normal emission at room temperature with a non-monochromatized Mg Kα X-ray source (1253.6 eV). Single spectra were acquired using 0.1 eV steps, 0.5 s collection time, and 20 eV pass energy. In order to analyze the single components of the C 1s and N 1s regions, the spectra were separated into chemically shifted components. For the C 1s region, an asymmetrical shape was used for the sp<sup>2</sup> component, whereas symmetrical Voight functions were used for the sp<sup>3</sup> component and the C–O functional groups. For the N 1s region, symmetrical Voight functions were used.

#### 2.4. Electrochemical Characterization

Ex situ electrochemical characterization was conducted in a conventional three-electrode cell using a rotating disk electrode (RDE). A glassy carbon rod and an Ag/AgCl (KCl sat) electrode were used as counter and reference electrodes, respectively. Measurements were carried out in a 0.1 M KOH solution saturated in Ar or O<sub>2</sub> at room temperature. The working electrodes were prepared by drop-casting. A catalyst ink was prepared by mixing 1 mg of catalyst and 10 µL of Nafion dispersion (5 wt.%, Sigma-Aldrich, Milan, Italy) in 500 µL of ultrapure water (Millipore Milli-Q system). An aliquot of 15 µL of the suspension was deposited onto a 3 mm diameter glassy carbon disk. First, cyclic voltammograms (CVs) were recorded in Ar- and O<sub>2</sub>-saturated electrolyte. Subsequently, linear sweep voltammograms (LSVs) were recorded at different rotation rates at 10 mV s<sup>−1</sup> in O<sub>2</sub>-saturated 0.1 M KOH. The electron number (n) transferred during the reaction was calculated employing the Koutecky–Levich formalism.

#### 2.5. In-Line Photoemission and Electrochemical Measurements

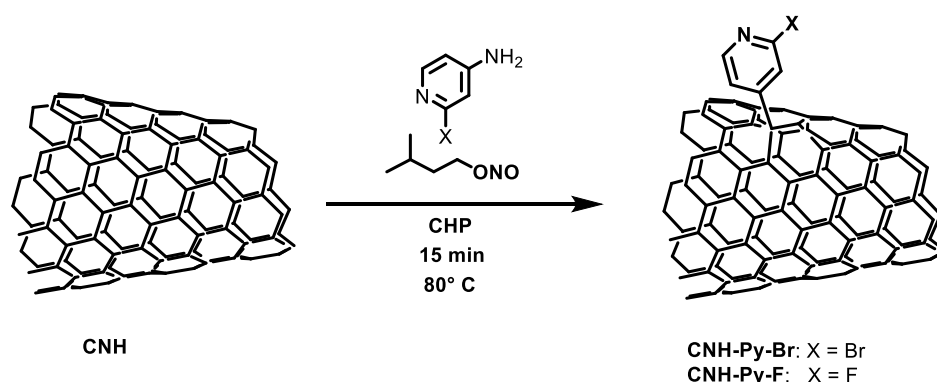
Measurements were performed in an ultrahigh vacuum (UHV) system that consists of two independent UHV chambers, the analysis (XPS) and the electrochemical (EC) chambers, connected through a transfer system. The UHV-EC transfer system, which consists of two manipulators (horizontal and vertical), is connected to the main preparation chamber through a gate valve. The horizontal manipulator is used to transfer the sample from the analysis chamber to the EC chamber, whereas the vertical one allows the sample to be raised to couple it to the electrochemical cell, which is connected to the EC chamber from the top. A custom made PEEK (polyether ether ketone) cell was used for the electrochemical measurements. A Pt wire was used as counter electrode and an Ag/AgCl/Cl<sup>−</sup> (3M KCl)

electrode placed in a Luggin capillary was used as reference electrode. A 0.1 M KOH solution, prepared from high purity reagents (Sigma-Aldrich) and saturated in Ar or O<sub>2</sub>, was used as the electrolyte. The electrolyte was pumped into the EC cell through a tubing system using a syringe pump (N-1010, Pump Systems Inc., Farmingdale, NY, USA), which allows for an accurate control of the flow. The electrolyte inlet consists of a capillary tube (diameter ca. 0.35 mm) placed in the center of the cell, whereas the outlet is constituted by eight holes (diameter 0.5 mm) placed around the central capillary. Prior to the EC measurements, the tubing system was purged with Ar to remove the oxygen and then, it was filled with the electrolyte. All the experiments were carried out at RT using a flow rate of 1 mL min<sup>−1</sup>. First, CVs were recorded in a small potential window (−0.6 V to +0.2 V vs. Ag/AgCl) to identify the working potentials and, subsequently, chronoamperometric curves were recorded at those potentials for 1200 s. The potentials studied were −0.1 V, −0.35 V, and −0.6 V vs. Ag/AgCl. After each EC treatment, the sample was transferred back to the analysis chamber to determine the chemical changes induced by the electrochemical work using XPS. Photoemission data were obtained as described above using the non-monochromatized Al K $\alpha$  X-ray source (1486.7 eV) and using 0.1 eV steps, 0.5 s collection time and 20 eV pass energy.

### 3. Results and Discussion

#### 3.1. Synthesis and Physicochemical Characterization of CNH Derivatives

Following the previously reported CNH functionalization procedure [26], we explored the possibility of synthesizing two CNH derivatives bearing different pyridyl moieties: CNH-Py-Br and CNH-Py-F (see Scheme 1).



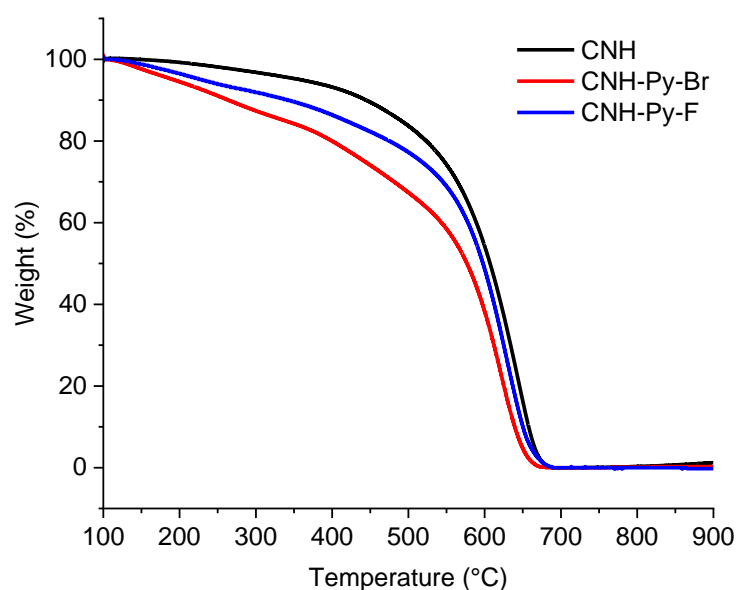


**Figure 1.** Overlay of the thermograms of pristine CNH (black), CNH-Py-Br (red), and CNH-Py-F (blue) in a nitrogen atmosphere.

The effective functionalization of CNH is confirmed by the concentration of stable solutions in  $\text{CHCl}_3$  (solubility: CNH-Py-Br = 1.4 mg/mL; CNH-Py-F = 1.1 mg/mL; see Section 2 for details), while pristine CNH did not afford stable solutions given the strong  $\pi$ -stacking interactions established within the individual CNH. Indeed, the organic moieties introduced with functionalization provide solubility to the nanostructure by limiting the tendency of CNH to aggregate.

Raman spectra of pristine and functionalized CNHs are reported in Figure 2. The ratio between the intensities of D ( $1320\text{ cm}^{-1}$ ) and G ( $1600\text{ cm}^{-1}$ ) bands are almost unaffected (D/G: CNH = 1/25; CNH-Py-Br = 1.23; CNH-Py-F = 1.15), indicating that the native structure of CNH is substantially preserved upon functionalization. In this sense, we can infer that the functionalization is high enough to improve dispersibility in liquid media, but also low enough to likely preserve electronic properties of the pristine carbon nanostructure.

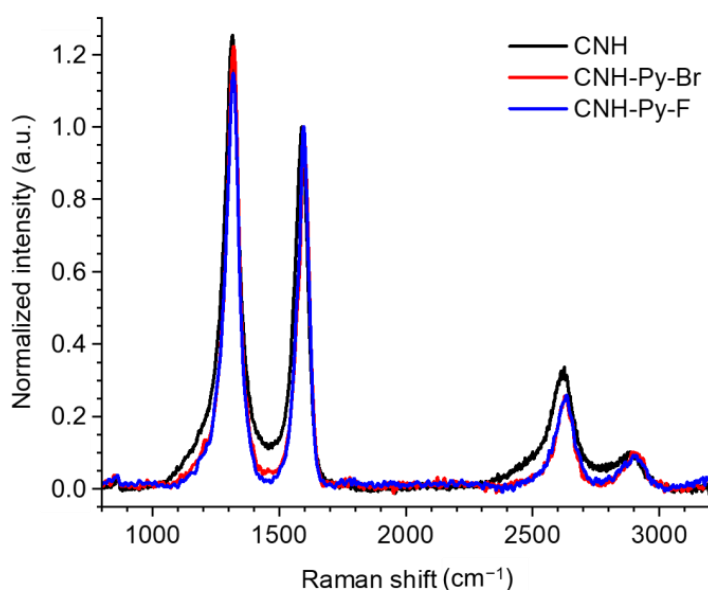


**Figure 2.** Raman spectra of pristine CNH (black), CNH-Py-Br (red), and CNH-Py-F (blue).

DLS analysis (Figure 3) provides an estimate of the solvodynamic diameter (SD) of the particles present in solution. SD values (CNH-Py-Br: 172 nm; CNH-Py-F: 88 nm) are compatible with the dimensions of functionalized CNHs [29] and suggest, in the case of CNH-Py-Br, the possible formation of a multilayered aryl coating expanding the size of the nanostructure, as previously observed with CNTs [27]. A radical process involved in the diazotization reaction may be responsible for both the growth of this coating and the loss of bromine, as suggested by XPS measurements (*vide infra*).

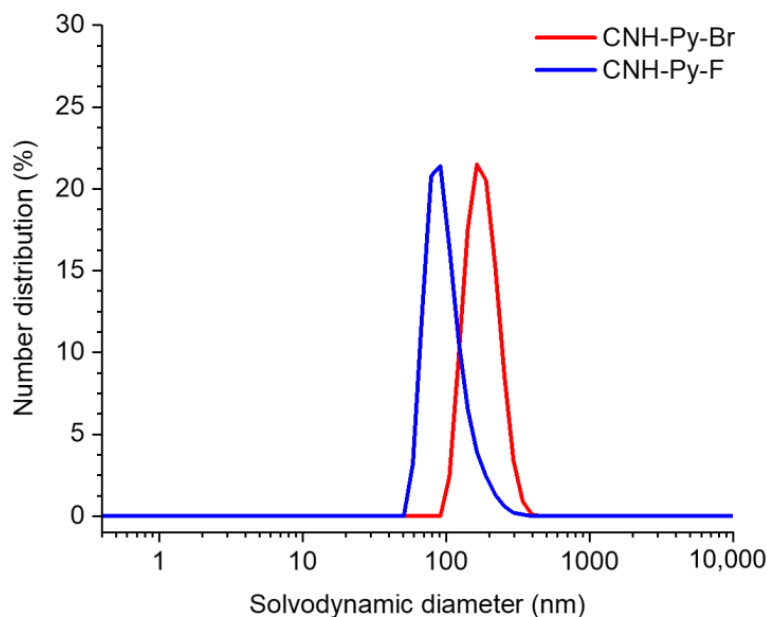


**Figure 3.** DLS analysis of CNH-Py-Br (red) and CNH-Py-F (blue).

The introduction and the nature of nitrogen, fluorine, and bromine species was investigated using XPS (Figure 4). Figure 4a shows the successful introduction of N species in both the CNH-Py-Br and CNH-Py-F samples. The analysis of the N 1s region shows that in addition to pyridinic N species at 398.7 eV, another three components at 399.7 eV, 401.2 eV, and 402.5 eV are also present. Unexpectedly, the main component is the one at 399.8 eV that could be attributed to azobenzene bonds formed through a diazo coupling reaction, as already observed for products of the Tour reaction [27]. However, it is more likely to assign this component to hydrogenated pyridinic N species formed under reaction conditions [31]. The component at 401.2 eV can be instead attributed to protonated pyridinic N species [31]. These results suggest therefore the sole presence of pyridinic N species (hydrogenated, protonated, or not), confirming the success of the functionalization process. Finally, the small amount of oxidized N species (<5 at.%) can be attributed to the oxidation of N species in contact with air [31].

The presence of the halogen was only confirmed for the CNH-Py-F sample, as shown in Figure 4b. The analysis of the F 1s region suggests two different fluorine environments. The component at lower binding energy can be associated with the 2-fluoropyridine moiety, while the one at a higher binding energy is ascribed to organic fluorine [13]. On the contrary, bromine was not detected in the CNH-Py-Br sample. This result could be attributed to radical addition mechanisms during the functionalization process, which could induce the breakage of the carbon–bromine bond.

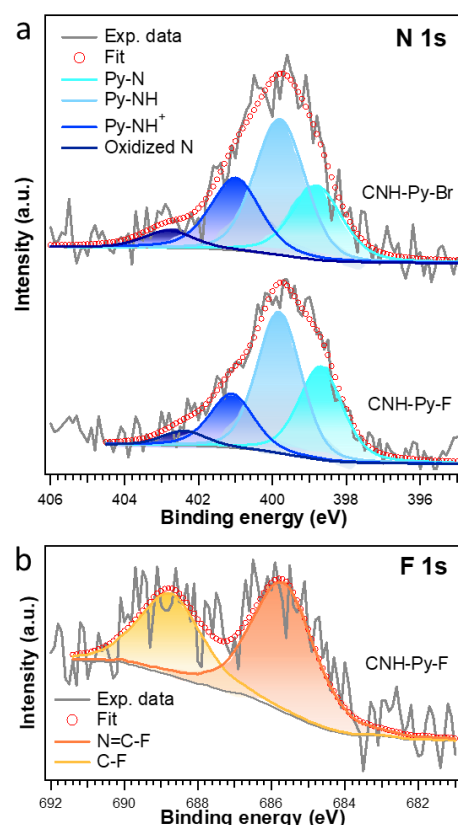


**Figure 4.** (a) N 1s XPS region of the CNH-Py-Br and CNH-Py-F samples, and (b) F 1s XPS region of the CNH-Py-F sample. The deconvolution into single chemical components is included in (a,b).

### 3.2. Electrochemical Characterization

The pristine and functionalized CNH were tested as metal-free catalysts towards the ORR. Figure 5a–c show the results obtained for the three materials. In Ar-saturated electrolyte, the currents observed were associated with the double layer of the carbon material, i.e., the charges accumulated on the electrode surface due to chemical and/or electrical interactions. However, in the presence of oxygen, a sharp negative current at around  $-0.3$  V vs. Ag/AgCl, attributed to the reduction of oxygen, was observed for all the materials. This value is similar to that reported in the literature for carbon materials [13,14], indicating that these materials are active towards the ORR. No differences in the onset potential were observed for the different functionalized samples (Figure 5g), although higher current densities were delivered by the functionalized materials, suggesting that the functional groups have an important effect on the activity of the materials.

In order to elucidate if the functionalization has any effect on the ORR mechanism, LSVs at different rotation rates were performed in  $O_2$ -saturated electrolyte. The results are reported in Figure 5d–f. By applying the Koutecky–Levich analysis, the number of exchanged electrons was determined (Figure 5h). Pristine CNHs mainly reduced oxygen to hydrogen peroxide since they show a value of  $n$  around two in the entire potential window studied. The functionalization of the CNHs favored the complete reduction of oxygen to hydroxyl ion, as deduced from the increase in the  $n$  values from two to four. No differences were observed for the two functionalized samples, suggesting that the change in the ORR mechanism from two to four electrons can be mainly attributed to the N species, and that the presence of fluorine has not a significant effect.



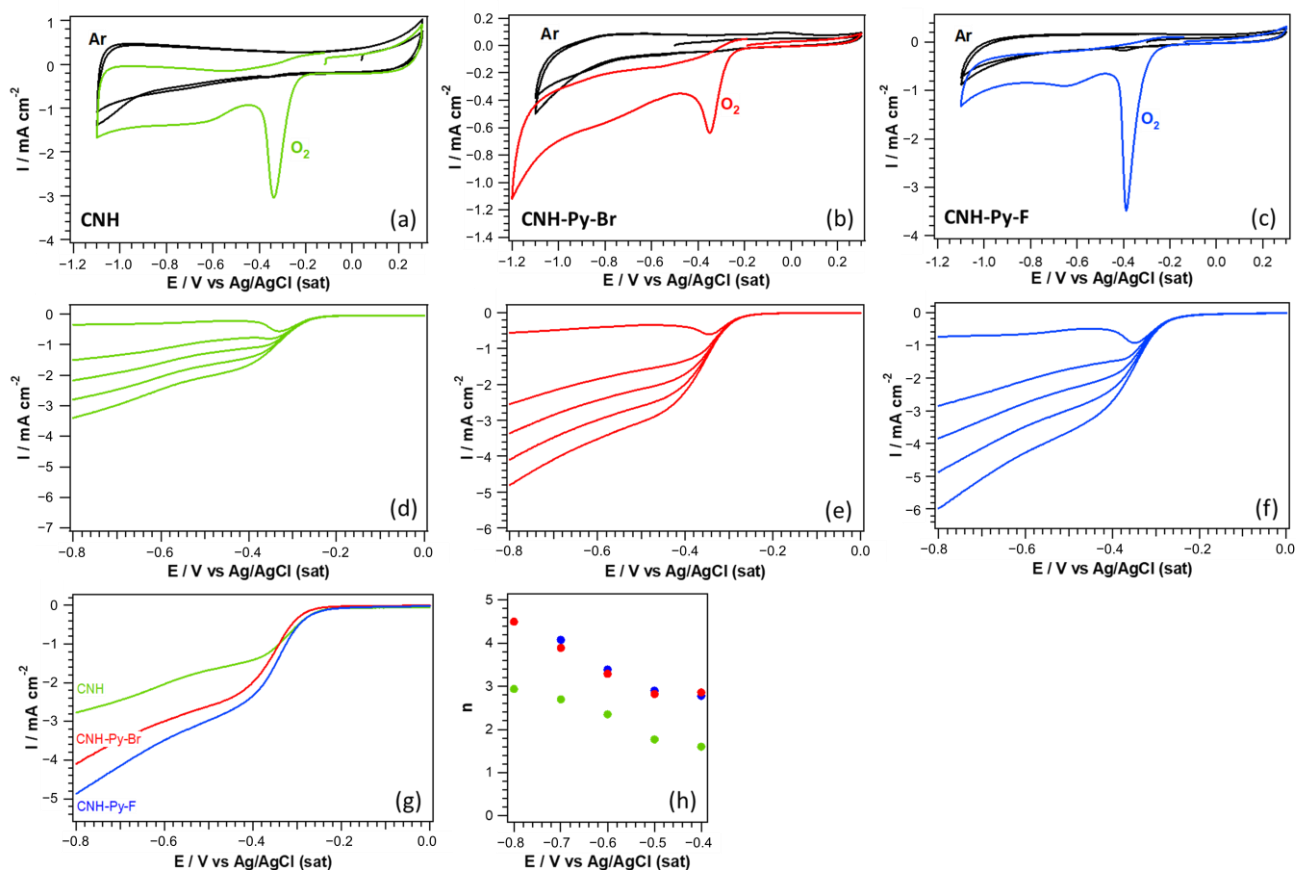


**Figure 5.** (a–c) Cyclic voltammograms recorded in Ar- and O<sub>2</sub>-saturated 0.1 M KOH; (d–f) linear sweep voltammograms recorded at different rotation rates in O<sub>2</sub>-saturated 0.1 M KOH; (g) comparison of the ORR activity at 1600 rpm; and (h) number of electrons exchanged as a function of the potential determined by the Koutecky–Levich analysis for the pristine CNH (green), CNH-Py-Br (red), and CNH-Py-F (blue) samples.

### 3.3. In-Line Photoemission and Electrochemical Measurements

In order to investigate the role of the functional groups and the active species involved in the ORR, we combined XPS and EC measurements to determine the changes undergone by the CNH-Py-F sample under ORR conditions. First, CVs in Ar- and O<sub>2</sub>-saturated electrolyte were performed in order to select the potentials of interest (Figure 6a). Three potentials were selected: −0.10 V (pre-catalytic conditions), −0.35 V (beginning of catalysis), and −0.60 V (catalytic conditions). Then, the sample was polarized at those potentials (Figure 6b), as detailed in Section 2.5. After each electrochemical treatment, the sample was analyzed by XPS.

Figure 6c shows the analysis of the N 1s photoemission line. The comparison of the spectra before and after the addition of Nafion shows the presence of a new component associated with N-F interactions and the increase in the protonated pyridinic component as well as the decrease in the pyridinic one. This result suggests an interaction between the N groups of the sample and Nafion. In particular, it has already been reported that pyridinic groups could preferentially interact with the F atom of Nafion, which would explain the decrease in this component and the increase in the N-F and protonated ones. This hypothesis agrees well with the data reported in the literature for the fluorination of N-doped carbon materials, where it has been demonstrated that the component at around 400.4–401.2 eV corresponds to the attachment of a fluorine atom in meta position to a pyridine-like nitrogen atom [32].

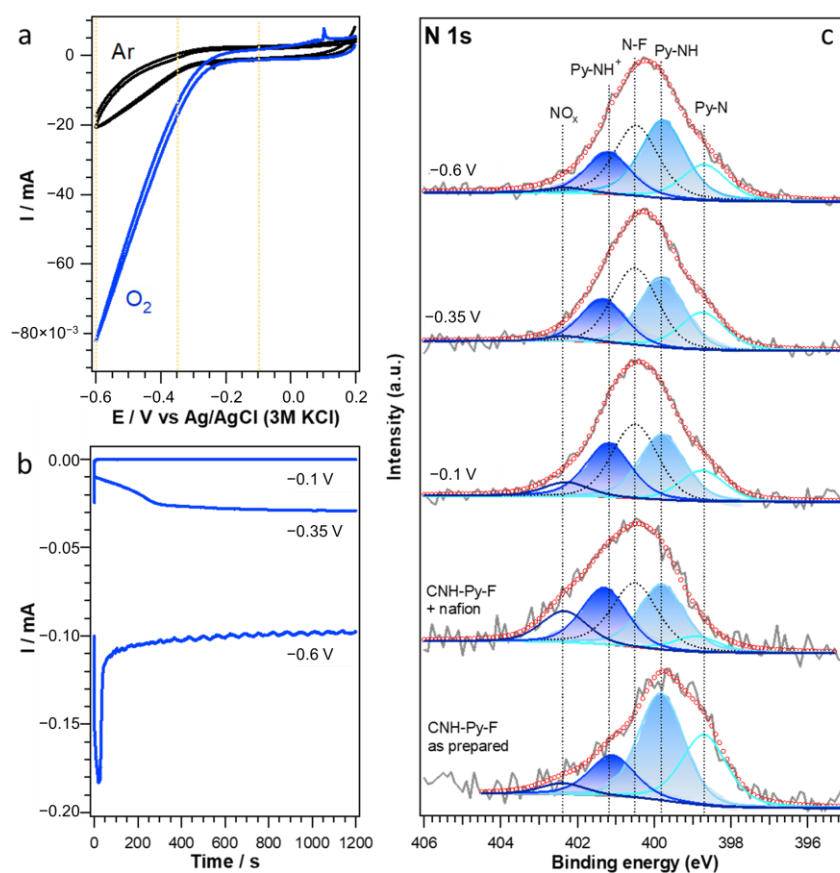


**Figure 6.** (a) Cyclic voltammograms recorded in Ar- and O<sub>2</sub>-saturated 0.1 M KOH of the CNH-Py-F in the XPS-EC cell; (b) current-time curves obtained at different potentials indicated in (a); and (c) deconvolution of the N 1s photoemission line in single-chemical components before and after the EC measurements.

Under precatalytic conditions, at  $-0.10$  V, no significant changes were observed, suggesting that the sample is stable under these conditions. Under catalytic conditions, on the contrary, as the potential decreased, the component associated with the NO<sub>x</sub> groups decreased, since they are reduced under ORR conditions. In addition, the hydrogenated N species (399.8 eV) increased, whereas the protonated ones (401.2 eV) decreased. The component associated with the N-F interaction remains unmodified in the whole range of potentials studied. The analysis of the N 1s region is reported in Table 1.

**Table 1.** Analysis of the single chemical components of the N 1s photoemission line for the CNH-NF sample before and after the EC measurements.

Sample	Py-N (398.6 eV)	Py-NH (399.7 eV)	N-F (400.4 eV)	Py-NH <sup>+</sup> (401.2 eV)	NO <sub>x</sub> (402.3 eV)
CNH-Py-F (as prepared)	31.7%	44.8%	---	18.4%	5.1%
CNH-Py-F + Nafion	5.6%	26.6%	30.7%	24.0%	13.1%
$-0.10$ V <sup>1</sup>	12.2%	28.9%	29.5%	22.6%	6.8%
$-0.35$ V <sup>1</sup>	17.2%	30.7%	29.1%	20.5%	2.5%
$-0.60$ V <sup>1</sup>	15.7%	33.9%	30.0%	18.1%	2.3%

<sup>1</sup> Potentials vs. Ag/AgCl.

In the literature, pyridinic N species have been mainly associated with the activity of the nitrogen-doped carbon materials [15,16], however, some other groups attribute the

activity of this type of materials to the graphitic N groups [17–19]. Therefore, there is still a big controversy in the literature with this regard.

Our results indicate that the protonated N species are reduced under ORR conditions to neutral NH species when oxygen is adsorbed on an adjacent carbon atom. This reduction explains the decrease in the protonated component (401.1 eV) and the increase in the hydrogenated one (399.8 eV). Therefore, the presence of protonated species favors the adsorption of oxygen, which is the initial ORR stage. The adsorption of oxygen on a carbon atom adjacent to the protonated N species is accompanied by the simultaneous reduction of such species, as suggested in the literature [33].

#### 4. Conclusions

In this work we synthesized N-doped carbon nanostructures by functionalizing CNHs with pyridine derivatives, respectively bearing a fluorine or a bromine atom in ortho position with respect to nitrogen, through a diazotization reaction. According to XPS analysis, bromine was lost during the functionalization process, while fluorine was retained. Three different pyridinic species (pyridinic, hydrogenated pyridinic, and protonated pyridinic N species) were present in the functionalized materials. The functionalized CNH derivatives were tested as metal-free ORR catalysts, and compared to pristine CNHs. The effective N-doping achieved in both derivatives enabled the complete reduction of oxygen affording hydroxyl ion, while hydrogen peroxide evolution was obtained with pristine CNHs. From the combined XPS–electrochemistry study, we found that protonated pyridinic N is the main N species involved in the ORR mechanism for our CNH derivatives, favoring the adsorption of oxygen in one adjacent carbon atom. However, the presence of fluorine did not induce any difference in the catalytic behavior. The participation of protonated pyridinic N species in the ORR process induces their reduction to hydrogenated pyridinic N species.

**Author Contributions:** Conceptualization, E.M. and S.A.; methodology, T.G. and L.C.; investigation, E.T., T.G. and L.C.; data curation, E.T., T.G. and L.C.; writing—original draft preparation, T.G., S.A., L.C. and E.M.; writing—review and editing, S.A., L.C. and E.M.; funding acquisition, L.C. and E.M. All authors have read and agreed to the published version of the manuscript.

**Funding:** Department of Chemical Sciences (project P-DISC#06BIRD2019-UNIPD) and “Centro Studi di Economia e Tecnica dell’Energia Giorgio Levi Cases” (project PRINTERS) of the University of Padua are gratefully acknowledged for their financial support. The authors would also like to acknowledge support from the Italian Ministry of Education, Universities, and Research (MIUR) through the program PRIN 2017–Projects no. 2017NYPHN8. T.G. also acknowledges the financial support of the European Research Council through the ERC StG project “JANUS BI” (grant agreement No. [101041229]).

**Institutional Review Board Statement:** Not applicable.

**Informed Consent Statement:** Not applicable.

**Data Availability Statement:** The data presented in this study are available in the article.

**Conflicts of Interest:** The authors declare no conflict of interest.

#### References

1. Ferriday, T.B.; Middleton, P.H. Alkaline fuel cell technology—A review. *Int. J. Hydrogen Energy* **2021**, *46*, 18489–18510. [[CrossRef](#)]
2. Vijayakumar, V.; Nam, S.Y. Recent advancements in applications of alkaline anion exchange membranes for polymer electrolyte fuel cells. *J. Ind. Eng. Chem.* **2019**, *70*, 70–86. [[CrossRef](#)]
3. Olabi, A.G.; Sayed, E.T.; Wilberforce, T.; Jamal, A.; Alami, A.H.; Elsaid, K.; Rahman, S.M.A.; Shah, S.K.; Abdelkareem, M.A. Metal-Air Batteries—A Review. *Energies* **2021**, *14*, 7373. [[CrossRef](#)]
4. Liu, Q.; Pan, Z.; Wang, E.; An, L.; Sun, G. Aqueous metal-air batteries: Fundamentals and applications. *Energy Storage Mater.* **2020**, *27*, 478–505. [[CrossRef](#)]
5. Zhang, L.; Li, L.; Chen, H.; Wei, Z. Recent Progress in Precious Metal-Free Carbon-Based Materials towards the Oxygen Reduction Reaction: Activity, Stability, and Anti-Poisoning. *Chemistry* **2020**, *26*, 3973–3990. [[CrossRef](#)] [[PubMed](#)]

6. Zhang, L.; Lin, C.Y.; Zhang, D.; Gong, L.; Zhu, Y.; Zhao, Z.; Xu, Q.; Li, H.; Xia, Z. Guiding Principles for Designing Highly Efficient Metal-Free Carbon Catalysts. *Adv. Mater.* **2019**, *31*, e1805252. [[CrossRef](#)] [[PubMed](#)]
7. Li, Y.; Tong, Y.; Peng, F. Metal-free carbocatalysis for electrochemical oxygen reduction reaction: Activity origin and mechanism. *J. Energy Chem.* **2020**, *48*, 308–321. [[CrossRef](#)]
8. Gao, R.; Dai, Q.; Du, F.; Yan, D.; Dai, L. C(60)-Adsorbed Single-Walled Carbon Nanotubes as Metal-Free, pH-Universal, and Multifunctional Catalysts for Oxygen Reduction, Oxygen Evolution, and Hydrogen Evolution. *J. Am. Chem. Soc.* **2019**, *141*, 11658–11666. [[CrossRef](#)]
9. Begum, H.; Ahmed, M.S.; Kim, Y.B. Nitrogen-rich graphitic-carbon@graphene as a metal-free electrocatalyst for oxygen reduction reaction. *Sci. Rep.* **2020**, *10*, 12431. [[CrossRef](#)]
10. Gao, Y.; Xiao, Z.; Kong, D.; Iqbal, R.; Yang, Q.-H.; Zhi, L. N,P co-doped hollow carbon nanofiber membranes with superior mass transfer property for trifunctional metal-free electrocatalysis. *Nano Energy* **2019**, *64*, 103879. [[CrossRef](#)]
11. Al-Hajri, W.; De Luna, Y.; Bensalah, N. Review on Recent Applications of Nitrogen-Doped Carbon Materials in CO<sub>2</sub> Capture and Energy Conversion and Storage. *Energy Technol.* **2022**, *10*, 2200498. [[CrossRef](#)]
12. Gutru, R.; Turtayeva, Z.; Xu, F.; Maranzana, G.; Thimmappa, R.; Mamlouk, M.; Desforjes, A.; Vigolo, B. Recent progress in heteroatom doped carbon based electrocatalysts for oxygen reduction reaction in anion exchange membrane fuel cells. *Int. J. Hydrogen Energy* **2023**, *48*, 3593–3631. [[CrossRef](#)]
13. Tuci, G.; Zafferoni, C.; Rossin, A.; Milella, A.; Luconi, L.; Innocenti, M.; Truong Phuoc, L.; Duong-Viet, C.; Pham-Huu, C.; Giambastiani, G. Chemically Functionalized Carbon Nanotubes with Pyridine Groups as Easily Tunable N-Decorated Nanomaterials for the Oxygen Reduction Reaction in Alkaline Medium. *Chem. Mater.* **2014**, *26*, 3460–3470. [[CrossRef](#)]
14. Wee, J.-H.; Kim, C.H.; Lee, H.-S.; Choi, G.B.; Kim, D.-W.; Yang, C.-M.; Kim, Y.A. Enriched Pyridinic Nitrogen Atoms at Nanoholes of Carbon Nanohorns for Efficient Oxygen Reduction. *Sci. Rep.* **2019**, *9*, 20170. [[CrossRef](#)]
15. Guo, D.; Shibuya, R.; Akiba, C.; Saji, S.; Kondo, T.; Nakamura, J. Active sites of nitrogen-doped carbon materials for oxygen reduction reaction clarified using model catalysts. *Science* **2016**, *351*, 361–365. [[CrossRef](#)]
16. Rao, C.V.; Cabrera, C.R.; Ishikawa, Y. In Search of the Active Site in Nitrogen-Doped Carbon Nanotube Electrodes for the Oxygen Reduction Reaction. *J. Phys. Chem. Lett.* **2010**, *1*, 2622–2627. [[CrossRef](#)]
17. Haque, E.; Zavabeti, A.; Uddin, N.; Wang, Y.; Rahim, M.A.; Syed, N.; Xu, K.; Jannat, A.; Haque, F.; Zhang, B.Y.; et al. Deciphering the Role of Quaternary N in O<sub>2</sub> Reduction over Controlled N-Doped Carbon Catalysts. *Chem. Mater.* **2020**, *32*, 1384–1392. [[CrossRef](#)]
18. Duan, Z.; Henkelman, G. Identification of Active Sites of Pure and Nitrogen-Doped Carbon Materials for Oxygen Reduction Reaction Using Constant-Potential Calculations. *J. Phys. Chem. C* **2020**, *124*, 12016–12023. [[CrossRef](#)]
19. Liu, R.; Wu, D.; Feng, X.; Müllen, K. Nitrogen-Doped Ordered Mesoporous Graphitic Arrays with High Electrocatalytic Activity for Oxygen Reduction. *Angew. Chem.-Int. Edit.* **2010**, *49*, 2565–2569. [[CrossRef](#)]
20. Kagkoura, A.; Tagmatarchis, N. Carbon Nanohorn-Based Electrocatalysts for Energy Conversion. *Nanomaterials* **2020**, *10*, 1407. [[CrossRef](#)]
21. Jung, J.Y.; Kim, S.; Kim, J.-G.; Kim, M.J.; Lee, K.-S.; Sung, Y.-E.; Kim, P.; Yoo, S.J.; Lim, H.-K.; Kim, N.D. Hierarchical porous single-wall carbon nanohorns with atomic-level designed single-atom Co sites toward oxygen reduction reaction. *Nano Energy* **2022**, *97*, 107206. [[CrossRef](#)]
22. Montiel Macias, E.; Valenzuela-Muñiz, A.M.; Alonso-Núñez, G.; Farías Sánchez, M.H.; Gauvin, R.; Verde Gómez, Y. Sulfur doped carbon nanohorns towards oxygen reduction reaction. *Diam. Relat. Mat.* **2020**, *103*, 107671. [[CrossRef](#)]
23. Bahr, J.L.; Yang, J.P.; Kosynkin, D.V.; Bronikowski, M.J.; Smalley, R.E.; Tour, J.M. Functionalization of carbon nanotubes by electrochemical reduction of aryl diazonium salts: A bucky paper electrode. *J. Am. Chem. Soc.* **2001**, *123*, 6536–6542. [[CrossRef](#)]
24. Fresco-Cala, B.; López-Lorente, Á.I.; Cárdenas, S. Monolithic Solid Based on Single-Walled Carbon Nanohorns: Preparation, Characterization, and Practical Evaluation as a Sorbent. *Nanomaterials* **2018**, *8*, 370. [[PubMed](#)]
25. Zięba, W.; Jurkiewicz, K.; Burian, A.; Pawlyta, M.; Boncel, S.; Szymański, G.S.; Kubacki, J.; Kowalczyk, P.; Krukiewicz, K.; Furuse, A.; et al. High-Surface-Area Graphene Oxide for Next-Generation Energy Storage Applications. *ACS Appl. Nano Mater.* **2022**, *5*, 18448–18461. [[CrossRef](#)]
26. Vicentini, N.; Gatti, T.; Salerno, N.; Hernandez Gomez, Y.S.; Bellon, M.; Gallio, S.; Marega, C.; Filippini, F.; Menna, E. Effect of different functionalized carbon nanostructures as fillers on the physical properties of biocompatible poly(L-lactic acid) composites. *Mater. Chem. Phys.* **2018**, *214*, 265–276. [[CrossRef](#)]
27. Salice, P.; Fabris, E.; Sartorio, C.; Fenaroli, D.; Figà, V.; Casaletto, M.P.; Cataldo, S.; Pignataro, B.; Menna, E. An Insight into the Functionalisation of Carbon Nanotubes by Diazonium Chemistry: Towards a Controlled Decoration. *Carbon* **2014**, *74*, 73–82. [[CrossRef](#)]
28. Vicentini, N.; Gatti, T.; Salice, P.; Scapin, G.; Marega, C.; Filippini, F.; Menna, E. Covalent functionalization enables good dispersion and anisotropic orientation of multi-walled carbon nanotubes in a poly(L-lactic acid) electrospun nanofibrous matrix boosting neuronal differentiation. *Carbon* **2015**, *95*, 725–730. [[CrossRef](#)]
29. Pagona, G.; Karousis, N.; Tagmatarchis, N. Aryl diazonium functionalization of carbon nanohorns. *Carbon* **2008**, *46*, 604–610. [[CrossRef](#)]
30. Gatti, T.; Manfredi, N.; Boldrini, C.; Lamberti, F.; Abboto, A.; Menna, E. A D- $\pi$ -A organic dye-reduced graphene oxide covalent dyad as a new concept photosensitizer for light harvesting applications. *Carbon* **2017**, *115*, 746–753. [[CrossRef](#)]

31. Artyushkova, K. Misconceptions in interpretation of nitrogen chemistry from X-ray photoelectron spectra. *J. Vac. Sci. Technol. A* **2020**, *38*, 031002. [[CrossRef](#)]
32. Bulusheva, L.G.; Okotrub, A.V.; Kudashov, A.G.; Yudanov, N.F.; Pazhetnov, E.M.; Boronin, A.I.; Abrosimov, O.G.; Rudina, N.A. Fluorination of multiwall nitrogen-doped carbon nanotubes. *Russ. J. Inorg. Chem.* **2006**, *51*, 613–618. [[CrossRef](#)]
33. Takeyasu, K.; Furukawa, M.; Shimoyama, Y.; Singh, S.K.; Nakamura, J. Role of Pyridinic Nitrogen in the Mechanism of the Oxygen Reduction Reaction on Carbon Electrocatalysts. *Angew. Chem.-Int. Edit.* **2021**, *60*, 5121–5124. [[CrossRef](#)]

**Disclaimer/Publisher’s Note:** The statements, opinions and data contained in all publications are solely those of the individual author(s) and contributor(s) and not of MDPI and/or the editor(s). MDPI and/or the editor(s) disclaim responsibility for any injury to people or property resulting from any ideas, methods, instructions or products referred to in the content.